Tailoring Motif and Channel Terminating Groups of Conventional Copper MOFs for Their Enhanced Activity, Selectivity and Stability toward Electro-reduction of CO_2 to Hydrocarbons

Nusrat Rashid[1,4], Farooq Ahmad Dar[2,3], Mohsin Ahmad Bhat*[3], Pravin P. Ingole*[1]

[1] Department of chemistry, Indian Institute of Technology Delhi, New Delhi, 110016, India.
[2] Government Boys Higher Secondary School Trehgam, Kupwara, 193224, India.
[3] Department of Chemistry, University of Kashmir, Srinagar, 190006, India.
[4]Institute for Materials Discovery, University College London, London, WC1E7JE, United Kingdom.

Abstract

Judicious tuning of electronic effects, chemical functionalities, and type and distribution of active sites is a promising strategy to manage the selectivity, efficiency and electrochemical stability of electrocatalysts toward electrochemical reduction of CO_2 (ERCO2). Herein, we report a simple post-synthetic-modification to tune electronic effects and Lewis basicity in the copper based 3D and 2D metal organic frameworks (MOFs) involving chemical transformation of the free -COOH/-OH groups into amide/amine groups that improves their electrocatalytic stability and performance for hydrocarbon production. Detailed structural and voltametric characterizations reveal the unique electronic and structure-enhancing effects in the modified MOFs (especially in 2D MOF) endow them with excellent electrocatalytic performance (Overall Faradaic Efficiency (FE) 81%, with FEC1 = 62% and FEC2 = 19%) and stability toward ERCO2 (>4 hours). The significantly high FE for production of hydrocarbons over the modified MOFs is attributed to the improved Lewis acidity of the open metal centers and confined pores resulting in alternate active sites for *CO adsorption, hydrogenation and C-O bond dissociation.

Keywords: CO_2 reduction, Post Synthesis Modification, Cu MOFs, Hydrocarbon production, MOF structural stability.

**Corresponding authors:*

[1]PPI: Tel.: +91(11)26597547; E-mail: ppingole@chemistry.iitd.ac.in,*

[3]MAB: Tel.: +91(194)3565350; E-mail: mohsin@kashmiruniversity.ac.in*

Introduction

Metal-organic frameworks (MOFs) are turning out as promising materials for catalytic, photocatalytic, electrocatalytic and photo-electrocatalytic applications.[1-6] This is in view of their uniquely porous but very robust structure, bestowed with an ability to accommodate variedly balanced redox active metal centers and easy to functionalize organic linkers[7] that can be precisely tuned for desired catalytic applications.[1,2] Recent reports have demonstrated that MOF based materials exhibit excellent electrocatalytic activity especially toward electrochemical reduction of CO_2 (ERCO2).[8-12] However, the low intrinsic conductivity, spatial separation of metal centers by distances exceeding the tunneling range of electrons, and the low electrochemical/chemical stability of MOFs[13–15] especially in aqueous media are some serious concerns that hinder their large-scale exploitation for electrocatalysis. Approaches like calcination [16-19], chemical/electrochemical transformation of MOFs[3–5] and their hybridization with appropriate support materials/redox mediators [20-24] have been tested to address these concerns associated with ERCO2 performance of MOFs. However, most of these approaches either add up to the cost and complexity of the associated processes or often result in production of hybrid materials that lack the unique structural/functional aspects of the parent MOFs. Insertion of specific chemical functionalities into MOF networks via post-synthetic chemical and electrochemical treatments is advocated as a promising approach to tune their catalytic/electrocatalytic performance. [25-27]

Among various MOFs, the CuMOFs have been reported to offer higher yields of hydrocarbons and oxygenates in ERCO2. Copper-1,3,5-benzenetricarboxylate (CuBTC) MOF used in innate or modified form for ERCO2 [28-30] has been reported to yield oxalic acid in DMF, and methane, methanol, and formic acid in aqueous electrolyte solutions. Decoration of Coper-1,4-benzenedicarboxylate (CuBDC) MOFs over nanostructured carbon, metal[31] or metal oxide[32] supports has been demonstrated to increase the ERCO2 performance of MOFs and especially their selectivity to favor the production of hydrocarbons like CH_4 and C_2H_4. However, lower than desired electrochemical stability and electrocatalytic efficiency toward ERCO2, and significant HER performance of the so far reported CuMOF composites is a major concern limiting their use in bulk scale ERCO2 applications.[19] Approaches like ligand rigidification, ancillary ligand modification, and functionalized organic linkers have been reported to be very effective for improving the ERCO2 activity[23] of CuMOFs. However, majority of the chemical approaches suggested so far in this regard have been observed to result in embedded metal centers and/or insertion of electronically less conducting voluminous organic groupings into the MOF network. These changes besides decreasing the electronic conductivity and metal assisted ERCO2 performance of the MOFs, often raise serious concerns about the stability and selectivity issues of these chemically modified MOFs in practical applications. Through present work

we hereby communicate a simple, easy to carry, two-step chemical post-synthetic modification (PSM) approach for modifying the free -COOH/-OH groups on the 3D CuBTC and 2D CuBDC MOFs with amide/amine groups that demonstrate significantly improved electrochemical stability and performance of Cu-MOFs toward CO_2 while suppressing their hydrogen evolution reaction (HER) activity. The modified MOFs, particularly 2D CuBDC-Amide, exhibit a high faradaic efficiency (FE) for hydrocarbon production during electro-reduction of CO_2 with HER of just 19% even at -0.7 V (RHE). We believe that the work presented herein shall open a window for post synthetic modification of MOF motif and channels via simple chemical routes that can prove very effective to address the stability, activity and selectivity issues associated with the use of MOFs as ERCO2 electrocatalysts.

Results and discussion

Synthesis and Characterization of Materials

The channel linings as well as the nano/mesopores in CuBDC and CuBTC MOFs are terminated with -COOH or -OH groups of the organic linkers.[33] Chemical functionalization of these groups offers a promising means to tune the Lewis acidity, and hence the pore confinement of the MOF structure.[34] Intelligently conceived and appropriately executed such modifications can synergistically improve the electron-transfer characteristics of the metal sites of MOFs. Inspired with this idea, we conceived a simple route to bring about amide/amine modification of Cu-BTC/BDC MOF channel liners employing the “dateless” organic chemistry approach for the conversion of acid to amides via production of acid chlorides.[35] The schematic 1 illustrates the synthesis and amide functionalization steps for CuMOFs.

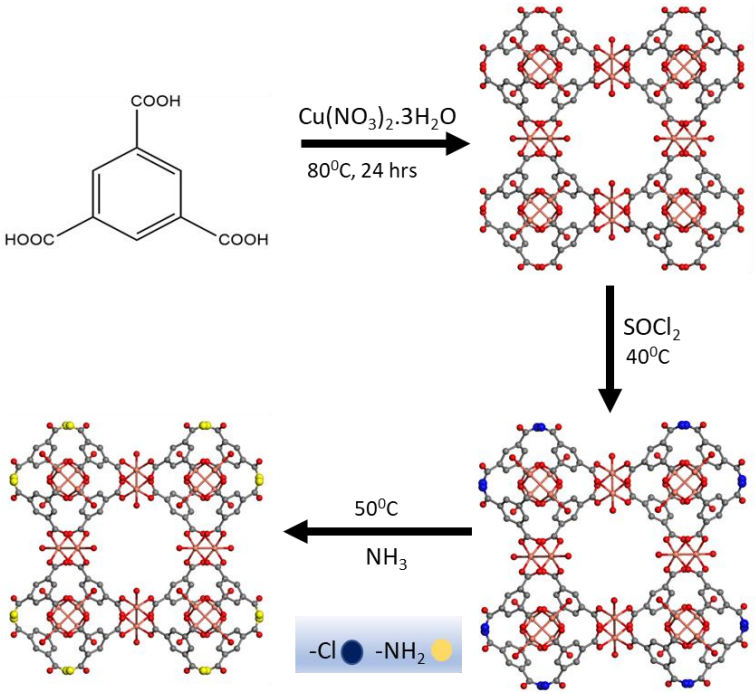

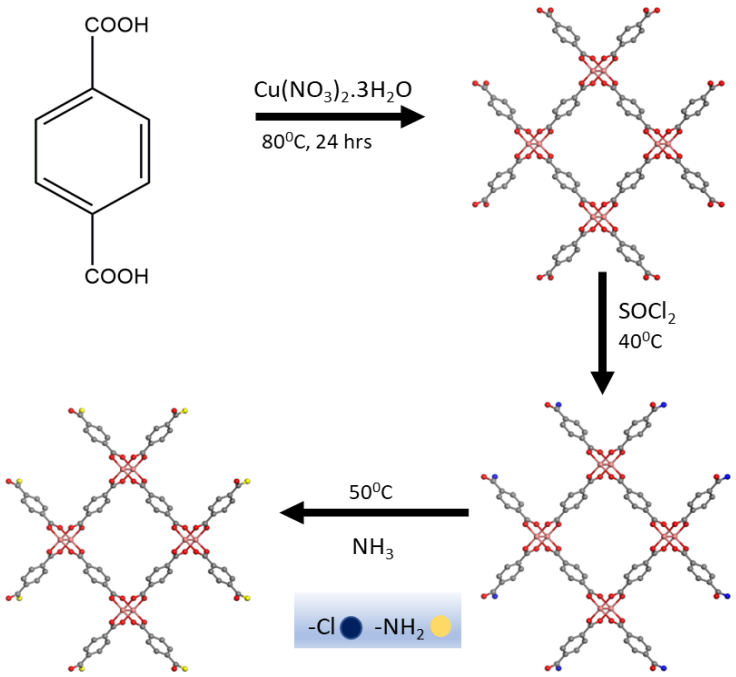

Schematic 1: An illustration of steps for the synthesis and its post-synthesis modification of (upper panel) CuBTC MOF, and (lower panel) CuBDC MOF into their amide-derivatives. Black: carbon, red: oxygen, blue: Chlorine, and yellow: amine.

CuBDC and CuBTC MOFs were synthesized through hydrothermal method following a reported protocol with slight modifications [36] as detailed in ESI 1.1. Together, the as prepared MOFs are referred to as 'acid-MOFs', highlighting presence of -COOH functional group on the organic framework motif and as channel liners. For the amide/amine functionalization, CuBDC and CuBTC MOFs were treated with $SOCl_2$ followed by ammonia water. The CuBDC and CuBTC MOFs obtained after PSM were named as CuBDC-Amide and CuBTC-Amide, respectively. Together, the PSM subjected MOFs are referred as 'amide-MOFs' to highlight the presence of amide groups as channel liners and/or motif end groups.

The XRD patterns recorded for Cu MOFs are shown in Figure 1 (a and b). For CuBTC, it depict intense peaks at 6.6°, 9.44°, 11.76°, 13.71°, 15.14°, 17.30° and 19.23°, corresponding to (200), (220), (222), (400), (331), (511) and (440) crystalline planes, which is in good-agreement to reported literature.[37] For CuBDC, characteristic peaks at 9.1°, 10.4°, 15.7°, and 17.4° correspond to the reflections from (220), (222), (331), and (333), respectively[38-40] and suggest that the framework is completely de-solvated i.e. without any traces of chemically bound DMF. For the MOF-amide samples, a slight shift toward lower diffraction angles was noticed, which is attributed to the pore confinement and change in the d-spacing due to incorporation of relatively bigger $-NH_2$ groups in the channels.[25,41] Importantly, this shift is more pronounced for mesopore-specific peaks that clearly reflects a greatly enhanced degree of pore confinement in both Cu-Amide-MOFs. The narrowness and high intensity of

the XRD peaks reflects high crystallinity of the obtained MOFs. Besides, the absence of any new peaks in the XRD records of Cu-Amide-MOFs implies the retention of phase purity of the native MOFs.

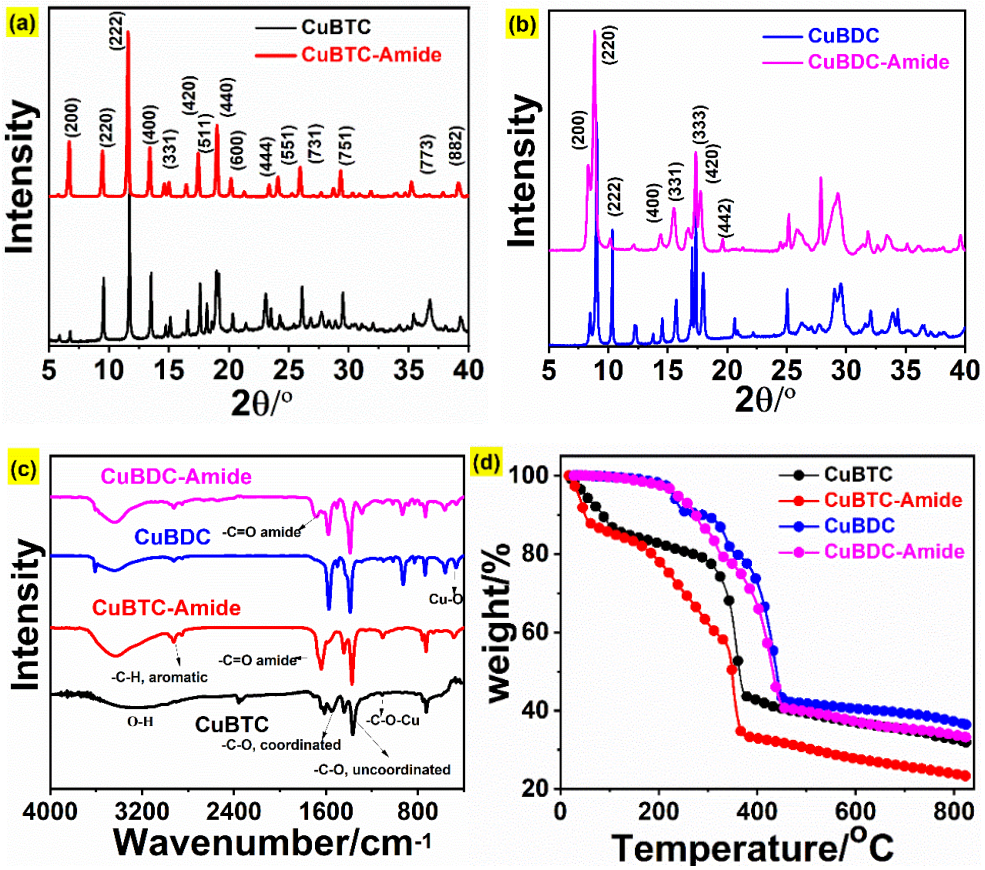

Figure 1: XRD patterns (a, b) showing crystal integrity unaltered on amine modification in both 3D and 2D MOFs, FTIR (c) showing functional groups on the acid and amide-MOFs, and TGA (d) showing the thermal stability (2D MOFs being more stable as compared to 3D MOFs in both acidic and amide form).

FTIR spectroscopy was employed to assess the changes in bonding pattern in acid-MOFs before and after their PSM transformation into respective amide-MOFs (Figure 1 (c)). The FTIR spectra for CuBDC and CuBTC show peaks at 2850-2950 cm^{-1} that represent aromatic -C-H stretching, at 1300-1400 cm^{-1} for uncoordinated -C-O vibrations, and at 1550-1600 cm^{-1} corresponding to the coordinated -C-O bond vibration.[42,43] The additional peak noticed at 1672 cm^{-1} for CuBTC-Amide and CuBDC-Amide-MOF corresponds to the -C=O amide stretching, and attests the modification of uncoordinated -COOH functionalities into amide groups. The broad bands noted at 3200-3400 cm^{-1} in the FTIR records of the CuBDC and CuBTC samples can be attributed to hydrated -OH groups of these MOFS [44]. Interestingly besides getting narrower, the intensity of this band increases significantly post-PSM of these MOFs. This feature noted in the FTIR spectra of CuBDC amide and CuBTC amide (especially the former) can be attributed to the overlapping of the -NH_2 characteristic IR bands and the -OH bands of these MOF networks [44,45]. The additional peak noticed at 1672 cm^{-1} for CuBTC-Amide and Cu-BDC

amide MOF corresponds to the -C+O amide stretching. These features, together with the XPS (as presented in the following sections), attest to the modification of uncoordinated -COOH functionalities into amide groups. Overall, the FTIR and XRD analysis for CuMOF and CuMOF-amide samples authenticates the grafting of Lewis active site, $-NH_2$, on the organic linker sites, via the conceived PSM. Thermal stability of the MOFs was ascertained through TGA measurements as shown in Figure 1 (d) that reflect good thermal stability of the native as well as amide CuMOFs. The initial weight losses observed in the range of 30-100^{0}C can be attributed to the evaporation of trapped water and DMF molecules. The loss of absorbed as well as the lattice or pore solvent molecules happens at higher temperatures (>200^{0}C). The presented thermal analysis besides establishing the significantly better thermal stability of CuBDC and CuBDC-Amide comparative to their CuBTC analogues, also suggest that amidation of CuBDC via PSM does not compromise its thermal stability. These observations suggest that structure of CuBDC and CuBDC-Amide (2D) is more rigid than their CuBTC-analogues (3D).

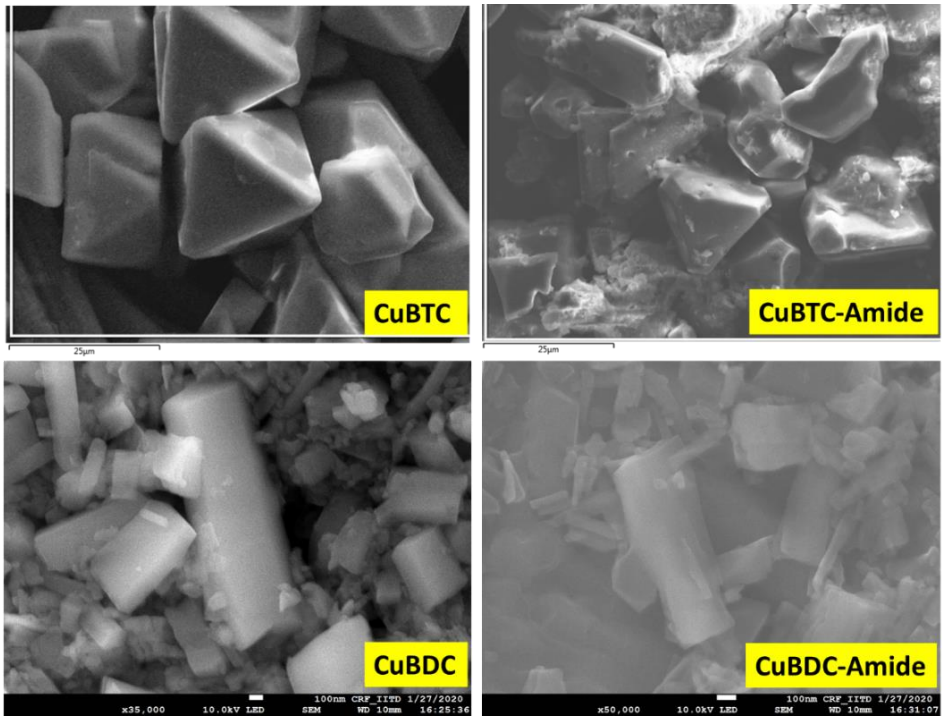

Figure 2: FESEM images of the acidic- and amide-copper Cu-MOFs showing octahedrons in CuBTC and CuBTC-Amide, and rectangular plates and rods in CuBDC and CuBDC-Amide. The microscopical topology has not changed on incorporation of amide functionalities.

The FESEM images of the MOF samples depicted as Figure 2 suggest well grown crystallites with smooth planes and edges. These images further suggest no marked change in the shape of native CuMOFs (especially for CuBDC) following their PSM transformation into amide analogues. The TEM images shown in Figure SI-1 also corroborate the similar findings. The EDX records over these

crystallites suggest a homogenous distribution of the elements Cu, C and O in CuBTC and CuBDC and additionally of N in the amide-MOFs (Figure SI-2, SI-3).

To assess the porosity and estimate the effective surface area of the CuMOFs, BET measurements were carried over the native and PSM-transformed CuMOFs. Figure SI-3 depicts the recorded BET isotherms, which follow type-IV isotherms typical to CuMOF materials. Figure 3 demonstrates the BJH plot with the average pore area for acidic and amide- CuMOFs, suggesting a decrease in average pore diameter by 29% post-transformation of CuBTC to CuBTC-Amide. Comparatively, the pore size seems to reduce by a much larger margin of ca. 51% when CuBDC is transformed to CuBDC-Amide (Table SI-1). Further, the BET analysis suggests a significantly enhanced specific surface area of amide-CuMOF as compared to that of acidic analogues. This implies the inclusion of amide/amine- groups within the channels that effects the neighboring pore environment. Smaller pores and narrower channels as suggested by the BET isotherms, lined with Lewis active sites (as suggested by FTIR analysis) would offer plenty of anchor points for the adsorption of CO2 and can act as secondary sites for further electron transfer concerted chemical reactions in the ERCO2.[46-48]

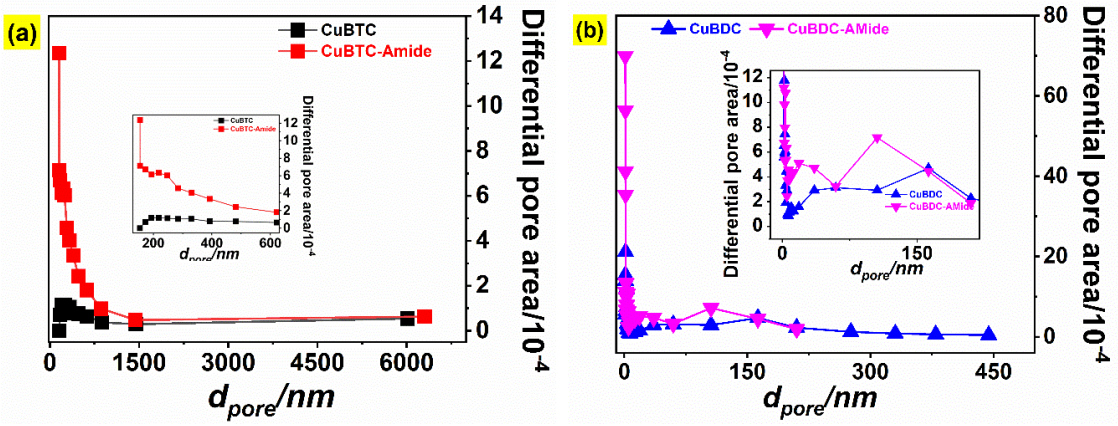

Figure 3: BJH plot with average pore area for acidic and amide- CuMOFs; (a) CuBTC and (b) CuBDC. (Inset figures) shift of average pore diameter from 218 nm to 154 nm and 42 nm to 20 nm in CuBTC-Amide and CuBDC-Amide, respectively

To quantify the composition and to establish the valence states of the constituent elements (Cu 2p, O 1s, C 1s, and N 1s) of the crafted MOFs, XPS analysis was followed as presented in Figure 4. In survey spectrum (Figure SI-5), a peak at 400 eV corresponds to the nitrogen (N 1s) present in Cu-Amide-MOFs. Both acidic and amide-MOFs suggested presence of Cu predominantly in 2+ state with a small amount present in 1+ state. The peak at 934.6 ± 0.2 eV agrees well with the literature reported values for Cu^{2+} in CuMOFs.[49,50] Further the careful analysis of the XPS measurements suggests that PSM transformation enhances the presence of Cu(I) as compared to Cu(II), as is reflected by the increasing of Cu(I)/Cu(II) ratio as well as decrease of satellite peak intensity associated with Cu(II). The presence of mixed oxidation states of copper, Cu(I) and Cu(II), have been reported in CuMOFs as metal

nodes of two independent pore structures.[51-53] These states have been observed to endow the MOF structures with increased stability towards moisture and increased CO adsorption, an intermediate of ERCO2, on Cu(I) sites without any substantial effect on the overall crystal properties. It is pertinent to mention here that the incorporation of such mixed states of Cu in CuMOFs usually requires high temperature treatments or addition of strong reducing agents. [52,53] However, our PSM approach not only enhances crystallinity and pore confinement but also results into mixed oxidation states of Cu in the MOF (Table SI-2) that is expected to significantly affect their electro-catalytic activity and stability. The amino functionalities are known as mild reducing agents as well as capping ligands and have been routinely used for the synthesis of metal nanoparticles. Thus, the increase in Cu(I)/Cu(II) ratio can be attributed to the amidation-treatment to the CuMOFs.

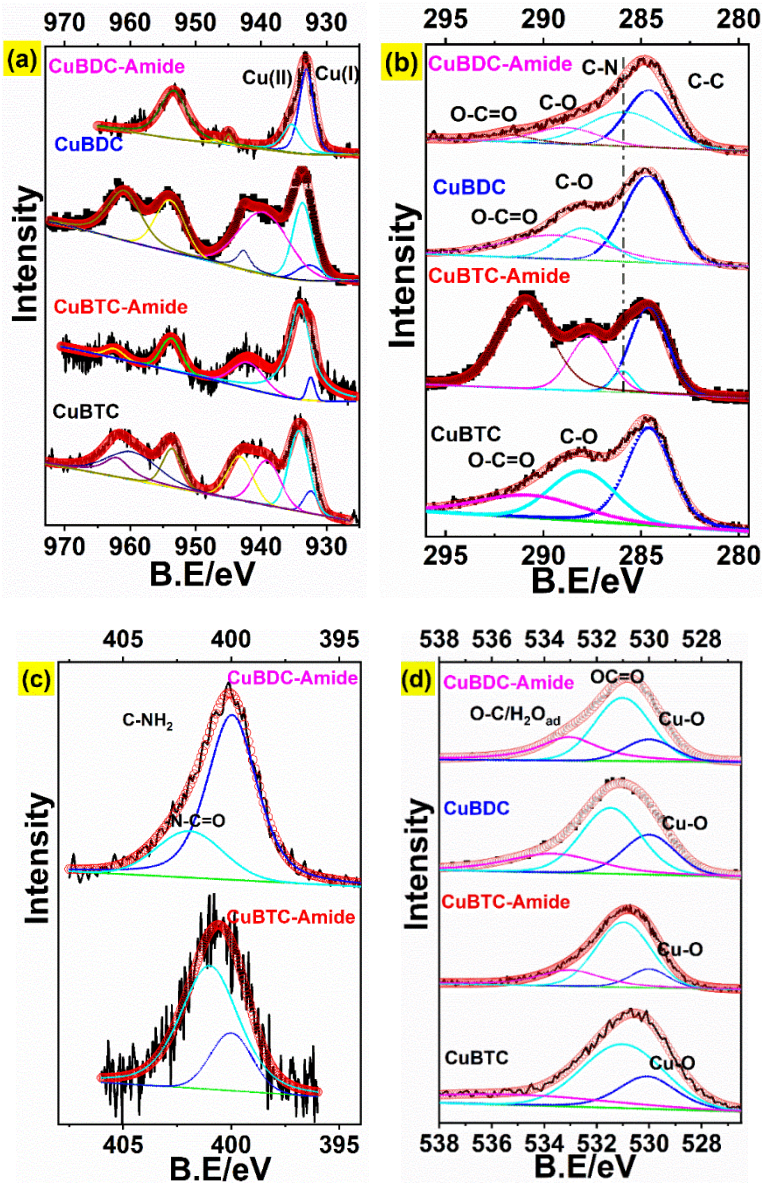

Figure 4: The core-level XPS spectra of CuMOFs corresponding to (a) Cu 2p, a slight shift (0.12 eV) on amidation of 2D MOF, (b) C 1s, a C-N bond feature visible in amide-MOFs, (c) N 1s, two N-

functionalities (amide and amine) inserted in the MOF channels and at motif terminations, and (d) O 1s metal-oxygen bonds as main coordination bridges with ligands.

Detailed N 1s spectra offered further insights into the type of functionalization of Cu-MOFs post their transformation via the attempted PSM. The XPS data suggest that for both CuBDC and CuBTC MOFs, the PSM conceived and attempted in the present work results in nitrogen functionalization of -COOH group to yield amide (401 eV) or to -OH terminating group to form amine (399 eV) functionalities.[54,55] Further, our XPS records clearly rule out the nitrogen functionalization as ancillary ligands, as it could have led to masking of the active copper site for Cu metal. The XPS peak at 529 eV in the O 1s spectra further confirms Cu linkages with O only in the native as well as amide-MOFs. A peak at 531.2 eV in the XPS records corresponds to C=O group. From the C 1s detailed spectra, peaks for C-C, C=O, O-C=O are observed in acidic-CuMOFs while in addition to these peaks, C-N peaks are observed in amide-CuMOFs.[56] Based on these observations regarding XPS records, it is safe to infer that except for amidation, the key linkages of MOF frameworks and the phase of CuBTC and CuBDC are not affected in any way by post-synthetic transformation procedure conceived and attempted in the present work.

Electrochemical reduction of CO_2 (ERCO2)

To assess the ERCO2 performance and electrochemical stability of the native and amide-MOFs, detailed voltammetric, impedance and bulk scale electrolysis investigations were carried in 0.2 M $KHCO_3$ electrolyte solutions in a custom designed 2-chambered electrochemical cell. Figure 5(a) depicts a sample set of linear sweep voltammetry (LSV) traces recorded in argon and CO_2 saturated solutions with MOF modified CFP as working electrode. The significantly higher currents noticed for the LSVs recorded under CO_2 than Ar saturated conditions suggest that both CuBTC and CuBDC MOFs are appreciably electrocatalytic for ERCO2. Further, these LSVs suggest less negative onset potential for ERCO2 over CuBDC MOF (-0.32 V) than over CuBTC MOF (-0.45 V vs. RHE) as well as higher current density for CuBDC than over CuBTC MOF at all potentials after the onset, implies a significantly better electrocatalytic performance by the CuBDC. Moreover, the amide-MOFs depicts lower onset potential and higher current density for ERCO2 than respective acid-MOFs, suggesting that the presented PSM significantly improves the electrocatalytic performance of the native MOFs toward ERCO2. Particularly, CuBDC-Amide-MOF demonstrates better ERCO2 performance than CuBTC-Amide-MOF. As the onset potential and current density are direct measure of the electrocatalytic performance, it can be inferred that PSM enhances the faradaic response to ERCO2 performance of CuBTC by 1.69 times, while enhancement by 2.61 times observed for CuBDC is way better. This was further attested by our EIS investigations carried over these MOF modified carbon fibre paper (CFP) surfaces.

Figure 5(b) show the Nyquist plots recorded at open circuit potential (OCP) over MOF modified CFP in CO_2 saturated 0.2 M $KHCO_3$ along with their simulated Nyquist plots, depicting lowest charge transfer resistance (R_{ct}) for amide-MOFs than their native analogues; CuBDC-Amide demonstrating the lowest R_{ct}. To assess the potential dependent electrocatalytic performance of the crafted MOFs toward ERCO2, EIS investigations were also carried at different applied potentials (Figure 5 (c) and (d)) chosen from the LSV records presented in Figure 5 (a). The EIS data fitted to the relevant circuits (Figure SI-6) clearly reflect a decrease in R_{ct} as the potential is shifted to more negative potentials, in agreement with the LSV records. Moreover, at all the potentials tested, R_{ct} for ERCO2 over amide-MOF was observed to be significantly lesser than their parent MOFs; lowest for CuBDC-Amide. Similarly, the contact resistance of amide-CuMOFs is noted as almost half the value than that observed for their acid-CuMOF analogues (Figure SI-6), indicating an increase in conducting properties of CuMOF post their amidation.

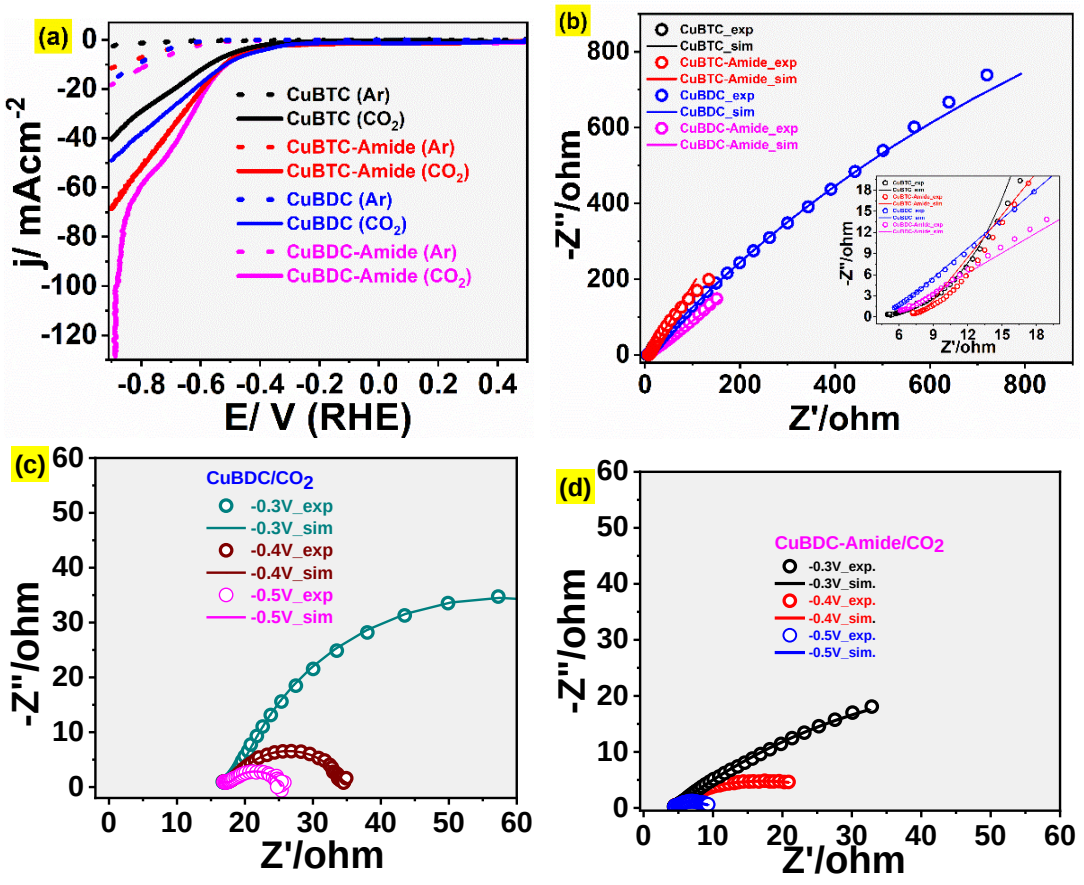

Figure 5: (a) LSV polarization curves in argon and CO_2 saturated 0.2 M $KHCO_3$, (b) Nyquist plot at OCP for acid-MOFs and amide-MOFs in CO_2 saturated 0.2 M $KHCO_3$. Nyquist plots for (c) CuBDC MOF and (d) CuBDC-Amide-MOF at different potentials in CO_2 saturated 0.2 M $KHCO_3$.

Product analysis and faradaic efficiencies

The product profiling and associated faradaic efficiencies (FE), and the electrochemical stability tests are a must to decide the practical utility of potential electrocatalysts for bulk scale ERCO2

applications. To assess the same for the MOFs crafted in the present work, bulk scale electrolysis investigations in two chamber electrolytic cells were carried under conditions similar to those employed for voltammetric and EIS investigations. Post the bulk scale electrolysis at different operational potentials (again, chosen from the LSV records presented in Figure 5 (a)) over MOF modified CFP surfaces, the gaseous and liquid products were collected and analyzed following the procedures detailed in the experimental section (ESI). The product analysis established the production of mainly H_2, C_2H_4, CH_3OH, HCOOH, CO, and CH_4. Averaged FEs for the different products, as estimated from a series of bulk electrolysis investigations, are presented in Figure SI-7, while the sum total of the FE at different operational voltages is presented as Figure 6. The estimated FEs for production of all ERCO2 products are noted to be dependent on the type of MOF, the potential employed for the electrolysis and the time scale of electrolysis. Importantly, an electrocatalytic performance of all the CuMOFs, native and amide-functionalized, toward ERCO2 seems to be much better than their HER activity that in turn is appreciably lesser in comparison to the HER reported on bulk Cu.[59,60]

The sum total of the FEs for ERCO2 products (Figure 6a) depicts predominant electro-production of hydrocarbons over amide-MOF surfaces in contrast to the acid-MOFs that favor the production of CO. ERCO2 over CuBTC-Amide and CuBDC-Amide surfaces produce CH_4, with FE of 28% and 32%, respectively, as the main product at -0.7 V. In contrast, the bulk electrolysis at -0.7 V over acidic-MOFs, i.e., CuBDC and CuBTC, generates CO as the main product with FE of 39% and 27%, respectively. This can be attributed to the ease of hydrogenation of the electro-produced CO over CuBDC-Amide and CuBTC-Amide-MOFs. While no traces of C2-hydrocarbons were noticed for ERCO2 over acid-MOFs, appreciable amounts of ethylene was noted over amide-MOF surfaces; CuBDC-Amide depicting highest FE (for ethylene) of ca. 18.9%. Importantly, the electrocatalytic performance of both 2D MOFs, CuBDC and its amide analogue, was noted to be better than that observed for 3D MOFs (CuBTC and CuBTC-Amide). Similar inferences reported in the recent past for 2D/3D MOF and covalent organic framework (COF) have attributed this to the lower accessibility of redox active sites in 2D networks and higher diffusional barriers in 3D networks. [59,60]

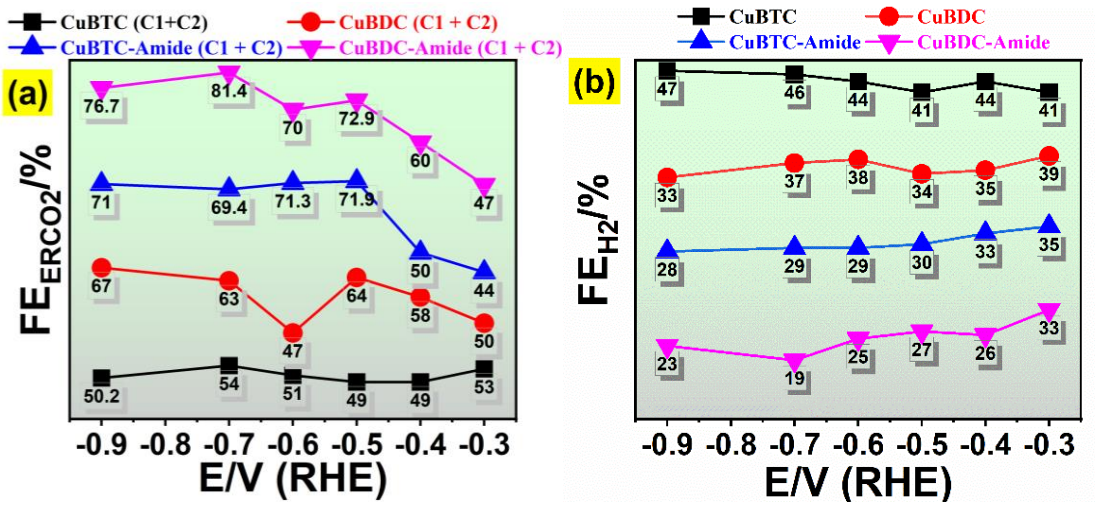

Figure 6: (a) Total FE for ERCO2 at different potentials, CuBDC-Amide-MOF with highest (81.4 %) efficiency and (b) HER FEs at different potentials for CuMOFs studied.

Another interesting factor for increased hydrocarbon production (mainly ethylene) on 2D amide-MOF could be assigned to the substantial presence of Cu(I) states available in its structure as part of metal node centers (suggested by the XPS data) than Cu(II) sites as compared to the acid-MOFs. Adsorption of ERCO2 intermediates, like CO, is expected to be better on Cu(I) sites than Cu(II)[53] due to possible back bonding from d^9 system of the former. Hence, the presence of Cu (I) sites is expected to result in longer residence time for CO intermediate and hence favoring the production of hydrocarbons over CO.[61,62] Such mixed sites have also been reported to favour CO_{bridge} intermediate formation which lead to production of hydrocarbons mainly methane and ethylene.[61] Figure 6 (b) suggest dominant ERCO2 performance of Cu-MOFs than their HER activity, except for CuBTC-Amide that shows comparable HER. Moreover, a shift of electrolysis voltages to more negative potential increases the electrocatalytic ERCO2 performance, reaching to a maximum at -0.7 V ± 0.1 V. At -0.7 V, CuBDC-Amide exhibit highest ERCO2 efficiency of 81.4% (C1 + C2 reduction products), followed by CuBTC-Amide (69.4%), CuBDC (63%) and CuBTC (54%). The lower activities by CuBTC acid-MOF are mainly attributed to structural degradation, less aqueous stability and less conductivity in comparison to CuBDC.[63-65] CuBTC being a 3D MOF, is more susceptible to aqueous degradation as compared to 2D CuBDC MOF.[66,67] In contrast, HER over acid-MOFs decreases initially till -0.5 V, the potential where surface degradation starts, but then slightly increases till -0.7 V. The higher ERCO2 performance of amide-MOFs than acid-MOFs could also be assigned to the presence of amine and amide group offering plentiful of active sites for CO_2 and CO adsorption, as is clearly attested by the LSV curves (Figure 5) exhibiting a CO* (* represents surface adsorbed species) related current plateau at -0.5 V to -0.69 V. This feature is most prominent especially in LSV records over CuBDC-Amide-MOF[68,69], the sample exhibiting the highest FE for hydrocarbon production.

Figure SI-7 (f) depicts the time dependence of HER performance observed for different MOF surfaces at applied potential of -0.7 V vs. RHE, where highest ERCO2 performance was noted. The depicted plots suggest that the HER activity of acid-MOFs increases as the electrolysis progresses, probably on account of Cu(II) to Cu(0) conversion and hence electro-reductive degradation (accompanied with surface reorganization and structure modification) of these MOFs when subjected to such high cathodic potentials. The HER performance of Cu(0) metal structures thus formed is expected to dominate their ERCO2 performance like that reported for copper clusters. Unlike acid-MOFs, negligible changes in the HER activity of amide-MOFs were noted when these were subjected to similar electrolyzing conditions.

Electrochemical Stability Investigations

In addition to the electrocatalytic performance, the electrochemical stability is an important factor to decide the practical utility of potential electrode materials. To assess the impact of presented PSM strategy over the electrochemical stability of CuMOFs, the MOF modified CFP surfaces were employed for ERCO2 at operational voltage of -0.7 V vs RHE for prolonged periods (4 hrs) and were analyzed to reveal changes if any in their morphology and composition. The FESEM images as depicted in Figure 7 suggest that post their use for ERCO2, morphology of acid-MOFs changes significantly. Comparatively, the SEM images of amide-MOFs, especially CuBDC-Amide, reflect an intact morphology. Figure SI-8 (a) and (b) depict typical XRD records for different MOF samples post their use for long term ERCO2. While MOF specific diffraction patterns seem to be largely retained by the amide-MOFs, the same is not true for acid-MOFs, implying appreciable structural integrity of amide-MOFs, and severe structural dis-integration of their acidic analogues post their use for ERCO2. Similar inferences are suggested by the XPS patterns recorded for these samples.

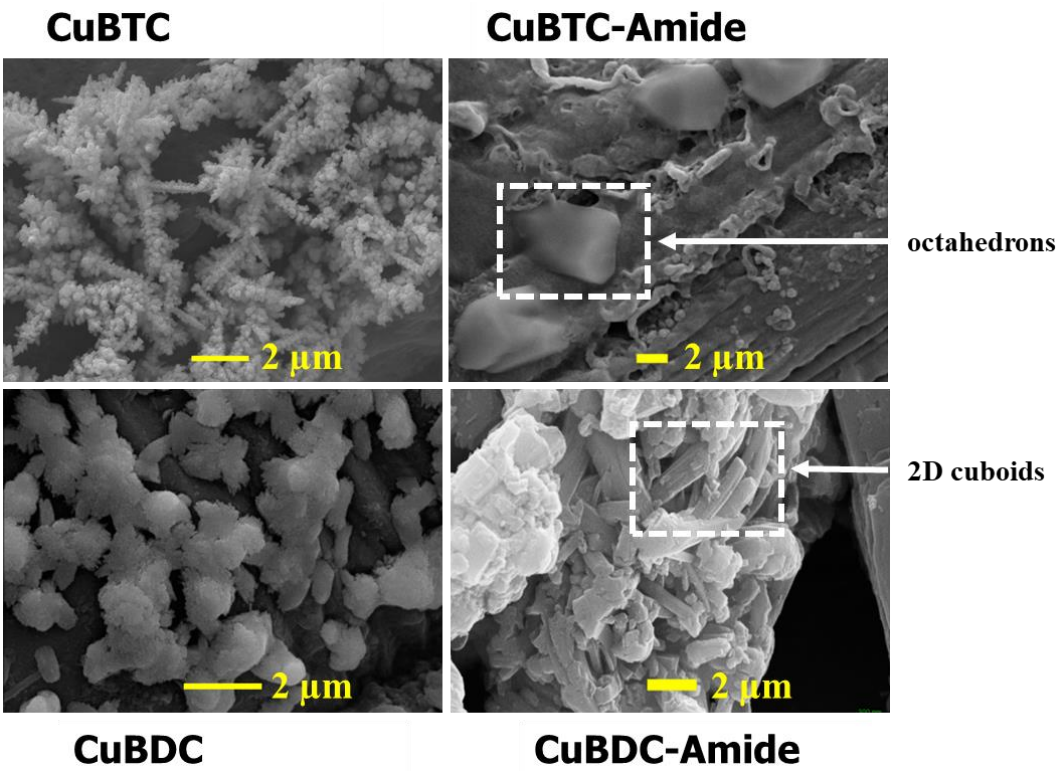

Figure 7: FESEM images of acidic- and amide- MOFs after 4-hour electrolysis showing negligible morphological degradation in the amide-MOFs as compared to the acidic-MOFs.

Figure 8 (a and b), depicts Cu 2p and N 1s specific XPS spectra recorded over CuMOFs post their use in ERCO2, which suggests that Cu is predominantly present as Cu(II) and Cu(I) in amide-MOFs, similar to their freshly prepared samples. Comparatively, the post ERCO2 XPS records for acid-MOFs show the presence of Cu(0). This implies that ERCO2 over unmodified CuMOFs results in a significant reductive loss of Cu(II) sites to Cu(0), that is expected to be accompanied by a collapse of organic framework as was also noted in their FESEM images. This Cu(II) to Cu(0) electro-reduction switched breakdown of unmodified CuMOF frameworks during CO_2 electrolysis, as suggested by the XRD, SEM, and XPS investigations, is responsible for the steep decrease in their ERCO2 activity and a rise in the HER activity as mentioned in the preceding section. Similarly, the N 1s XPS records suggest that amide-MOFs do not lose their nitrogen during ERCO2, further authenticating the electrochemical stability of these MOFs due to strong chemical bonding of nitrogen groups in amide-MOFs that ensure the structural stability and retention of the ERCO2 activity of amide-MOFs. This is in accordance with the post CO_2 electrolysis FESEM, XRD and XPS analysis.

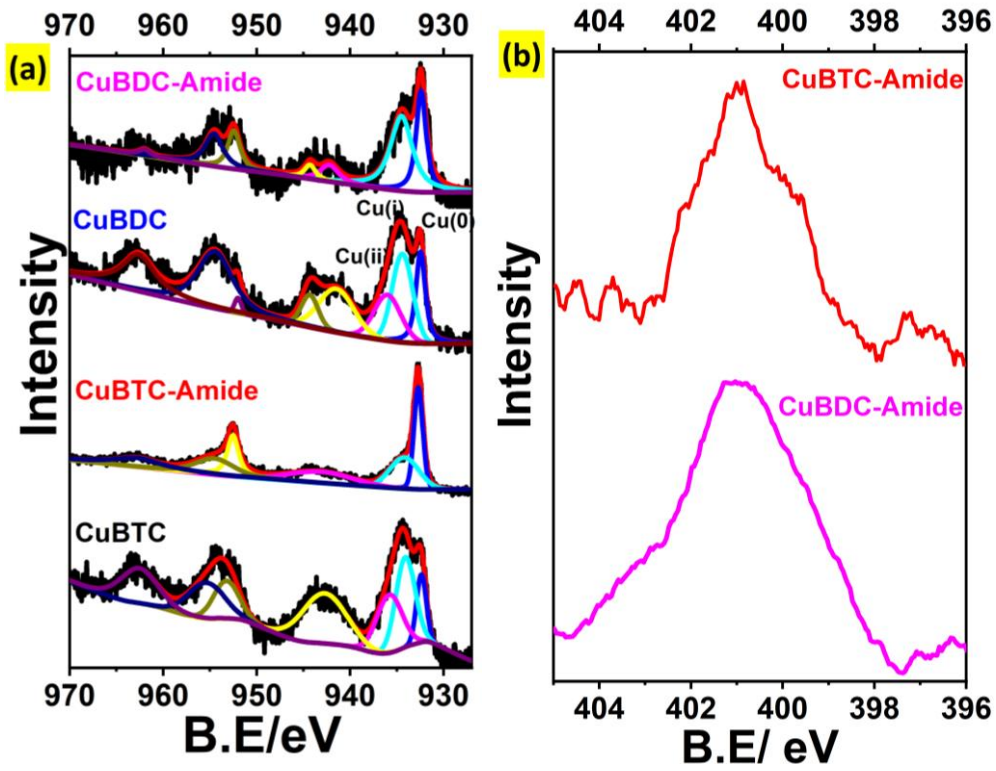

Figure 8: XPS of (a) Cu 2p of all CuMOFs, and (b) N 1s of amide-MOFs post-ERCO2 at -0.7 V (after 4-hour electrolysis under CO_2 atmosphere). The extra peak for Cu(0) in acidic-MOFs explains their structure degradation accompanying surface reorganization at highly reducible potentials of -0.7 V.

The amidation process also protects the metal center of these MOFs from getting reduced under highly reducing applied potentials. Contrarily, acid-MOFs lose their organic framework with time and yield metal clusters that are more active for HER than ERCO2. For example, as shown in Fig SI-10, the copper clusters into Cu (O) during CO_2 reduction and undergoes a permanent surface reorganization, but the same figure suggests that Cu sites in amide-MOFs do not undergo cluster formation, which can be due to the structure rigidification brought about by channel lined -NH_2 and -NH groups. The absence of Cu clusters can be also explained by the electron delocalisation from N-site from and to Cu [70], maintaining the overall structure. It is also well-known effect that there is always subsurface Cu(I) active sites which do not form Cu(0) clusters and have been identified as active sites [71]. Being Lewis bases, -NH_2 sites would facilitate the proton transfer coupled electro-reduction of CO^*, an intermediate of ERCO2. Besides, the close proximity of amide/amine sites to the CO production sites would favor the C-C bond formation and hence production of C2 hydrocarbons. The higher activity of CuBDC-Amide for production of hydrocarbons than CuBTC-Amide is well supported by type of surface functional group modification analyzed using XPS (Figure 4 (d)) that suggests presence of more -C-NH_2 groups as compared to -CO-NH_2 groups in the former. In view of the expected electron-delocalization effects in the amides, amine groups are expected to be more effective for production of the hydrocarbons. Moreover, the nitrogen groups in the framework seem to facilitate

the CO_2 uptake via their Lewis acid-base interactions and additionally stabilize the Cu(II) and Cu(I) cations of the amide-MOF framework. In past, two different effects of N-based ligands/functionalities have been reported for the ERCO2, (1) ligand centered reduction: the ligand is redox-active and can transfer electrons to the CO_2 or any intermediate[72,73], and (2) mixed redox process: where nitrogen-containing groups help in increasing electron density on the reduced metal center.[20,70] N-containing groups may also act as promoters by outer-sphere coordination effects, mass transport effects, and HER suppression.[73-76]

Schematic 2 illustrates the different possible roles of inserted amide/amine groups in PSM subjected CuMOFs that can be proposed to account for their enhanced ERCO2 activity and selectivity. -NH_2 functionalities can act as reactant deliverers following their Lewis acid (CO_2)—Lewis base interactions. This reactant transportation/storage ability of these sites shall lead to increased supply of reactant hence facilitation of ERCO2. As shown in schematic 2(b), -NH_2 groups being less electronegative than -COOH group can stabilize Cu (I)/Cu (II) states more efficiently. These groups can also act as alternate active sites by interacting with CO and aiding its hydrogenation and/or C-O bond dissociation as shown in schematic 2(b).

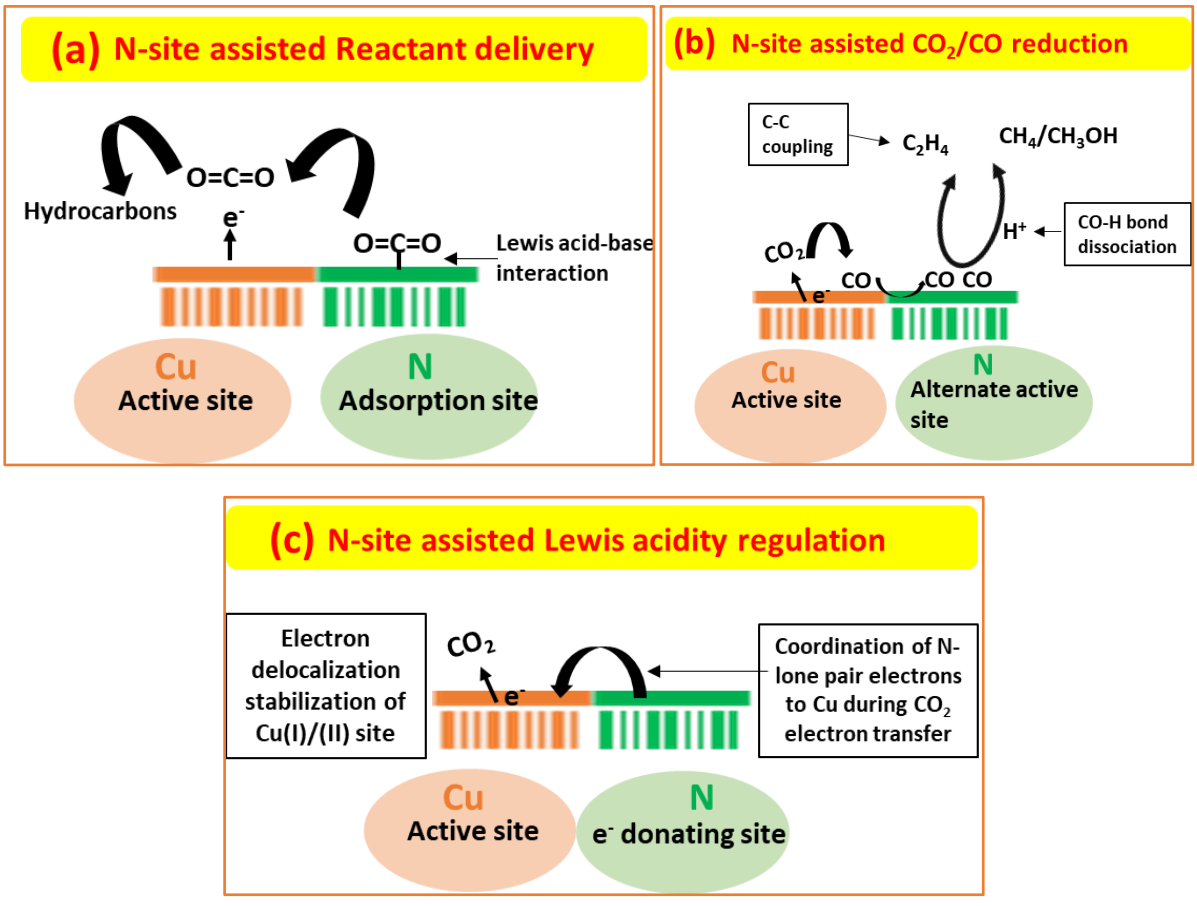

Schematic 2: Three different roles of inserted amide/amine groups in PSM CuMOFs for ERCO2 activity, selectivity, and stability. (a) N-assisted delivery of CO_2 at metal active center, (b) N-site assisted

CO_2/CO reduction in final products, thus acting as an alternate active site, and (c) Donation of available electron density on N-site to coordinate with Cu site during electron transfer from Cu to CO_2. Alternative active site for CO adsorption, protonation, and C-O bond dissociation.

The comparative enhancement noticed in the morphology retention, spectroscopic signatures, and the ERCO2 activity and stability of CuMOFs post their amide/amine functionalization via the proposed PSM, make us to conclude that;

(i) Presence of amide groups in the Cu-amide-MOFs stabilize the metal center of the MOF via execution of its electronic effect over the redox active metal centre (a positive shift of 0.12 eV occurs from CuBDC-Amide to CuBDC as evidenced in Cu 2p XPS peak).
(ii) Inclusion of amide functionality into CuMOFs, suppresses HER from 46% to 29% in CuBTC to CuBTC-Amide by increasing ERCO2 into hydrocarbons via its impact over electron transfer concerted hydrogenation and accelerated C-O bond dissociation. HER suppression was also found with CuBDC at 37% to 29% in CuBDC-Amide.

In view of these observations, it is safe to assume that the strategy conceived and executed for the modification of CuBDC and CuBTC MOFs in the present work, besides lowering their HER performance, significantly improves their electrochemical stability and activity toward ERCO2. Importantly the improvement in ERCO2 performance includes a preferential enhancement for production of hydrocarbons and lowered activity for CO production. It is pertinent to mention here that low HER activity, better and preferential production of hydrocarbons than CO are much sought features to qualify a material as a high-performance electrocatalyst for ERCO2.

Conclusions

A novel post-synthetic modification (PSM) strategy for chemical functionalization of channel lining in 2D and 3D CuMOFs was optimized. The CuMOFs were modified at free carboxylic groups on their organic framework with amide/amine groups without any structural and morphological changes. This PSM results in enhanced pore confinement, structural enhancement, electrochemical stability and electrocatalytic performance and selectivity of the CuMOFs toward electroreduction of CO_2 to hydrocarbons together with a suppression in their HER activity. The presented study opens scope for the design and development of new CuMOF based materials whose stability, activity, and selectivity towards ECR can be easily tuned and controlled for their as desired electrochemical stability and electrocatalytic performances.

Supporting Information

Methods and procedure. Characterization (TEM, EDX, BET, XPS, EIS, FE%) etc.

Acknowledgements

NR acknowledges CSIR-UGC for the fellowship. PPI thanks DST-SERB, Govt. of India for the financial support vide SB/EMEQ-339/2014 and EEQ/2020/00058 under the "Empowerment and Equity Opportunities for Excellence in Science". Authors are thankful to Central Research Facility (CRF) and Nanoscale research facilities (NRF) of IIT Delhi for assistance in material characterization. Authors thank Dr. Tokeer (Jamia Millia Islamia, New Delhi, India) and his students for assistance in BET measurements and Dr. Mostakim SK (Indian Institute of Technology Mumbai, India) for his insights in MOF structures and reaction engineering.

References

1. Lee, J. Y.; Farha, O. K.; Roberts, J.; Scheidt, K. A.; Nguyena, S. T.; Hupp, J. T. Metal–Organic Framework Materials as Catalysts. *Chem. Soc. Rev.*, **2009**, 38, 1450-1459. https://doi.org/10.1039/B807080F.
2. Wei, Y. S.; Zhang, M.; Zou, R.; Xu, Q. Metal–Organic Framework-Based Catalysts with Single Metal Sites. *Chem. Rev*. **2020**, 120, 21, 12089–12174. https://doi.org/10.1021/acs.chemrev.9b00757.
3. Wang, C. P.; Feng, Y.; Sun, H.; Wang, Y.; Yin, J.; Yao, Z.; Bu, H. B.; Zhu, J. Self-Optimized Metal–Organic Framework Electrocatalysts with Structural Stability and High Current Tolerance for Water Oxidation. *ACS Catal.* **2021**, 11, 12, 7132–7143. https://doi.org/10.1021/acscatal.1c01447.
4. Zhang, W.; Yu, Y.; Huang, R.; Shi, X. Efficient Photocatalytic Reduction of CO_2 to CO Using $NiFe_2O_4$@N/C/SnO_2 Derived from FeNi Metal–Organic Framework. *ACS Appl*. *Mater*. *Interfaces.* **2021**, 13, 34, 40571–40581. https://doi.org/10.1021/acsami.1c10147.
5. Amr, R.; Jin, H.; He, D.; Mu, S. Design Engineering, Synthesis Protocols, and Energy Applications of MOF-Derived Electrocatalysts. *Nano-Micro Letters*. **2021**, 13, 132. https://doi.org/10.1007/s40820-021-00656-w.
6. Li, X.; Zhu, Q. L. MOF-based Materials for Photo- and Electrocatalytic CO_2 Reduction. *EnergyChem*. **2020**, 2 (3), 100033. https://doi.org/10.1016/j.enchem.2020.100033.
7. Yi, J.D.; Xie, R.; Xie, Z. L.; Chai, G. L.; Liu, T. F.; Chen, R. P.; Huang, Y. B.; Cao, R. Highly Selective CO_2 Electroreduction to CH_4 by In Situ Generated Cu_2O Single-Type Sites on a Conductive MOF: Stabilizing Key Intermediates with Hydrogen Bonding. *Angew Chem Int Ed Engl*. **2020**, 59 (52), 23641-23648. doi: 10.1002/anie.202010601.
8. Zhong, H.; Ghorbani, M. A.; Ly, K. H.; Zhang, J.; Ge, J.; Wang, M.; Liao, Z.; Makarov, D.; Zschech, E.; Brunner, E.; Weidinger, I. M.; Zhang, J.; Kreshennikov, A. V.; Kaskel, S.; Dong, R.; Feng, X. Synergistic Electroreduction of Carbon Dioxide to Carbon Monoxide on Bimetallic Layered Conjugated Metal-Organic Frameworks. *Nat*. *Commun*. **2020**, 11 (1), 1–10. https://doi.org/10.1038/s41467-020-15141-y.
9. Zhao, M.; Huang, Y.; Peng, Y.; Huang, Z.; Ma, Q.; Zhang, H. Two-Dimensional Metal-Organic Framework Nanosheets: Synthesis and Applications. *Chem. Soc. Rev*., **2018**, 47, 6267-6295. https://doi.org/10.1039/c8cs00268a.
10. Zhang, H.; Nai, J.; Yu, L.; Lou, X. W. Metal-Organic-Framework-Based Materials as Platforms for Renewable Energy and Environmental Applications. *Joule*. **2017**, 1(1) 77–107. https://doi.org/10.1016/j.joule.2017.08.008.
11. Kornienko, N.; Zhao, Y.; Kley, C. S.; Zhu, C.; Kim, D.; Lin, S.; Chang, C. J.; Yaghi, O. M.; Yang, P. Metal-Organic Frameworks for Electrocatalytic Reduction of Carbon Dioxide. *J. Am. Chem*. *Soc*. **2015**, 137 (44), 14129–14135. https://doi.org/10.1021/jacs.5b08212.

12. Al-Rowaili, F. N.; Jamal, A.; Ba Shammakh, M. S.; Rana, A. A Review on Recent Advances for Electrochemical Reduction of Carbon Dioxide to Methanol Using Metal-Organic Framework (MOF) and Non-MOF Catalysts: Challenges and Future Prospects. *ACS Sustain. Chem. Eng.* **2018**, 6 (12), 15895–15914. https://doi.org/10.1021/acssuschemeng.8b03843.
13. Meng, D. L.; Zhang, M. D.; Si, D. H.; Mao, M. J.; Hou, Y.; Huang, y. B.; Cao, R. Highly Selective Tandem Electroreduction of CO2 to Ethylene over Atomically Isolated Nickel–Nitrogen Site/Copper Nanoparticle Catalysts. *Angew Chem Int Ed Engl*. **2021**, 60 (48), 25485-25492. https://doi.org/10.1002/anie.202111136.
14. He, C.; Liang, J.; Zou, Y. H.; Yi, J. D.; Huang, Y. B.; Cao, R. Metal-organic frameworks bonded with metal N-heterocyclic carbenes for efficient catalysis, *National Science Review*, **2022,** 9 (6), 157, https://doi.org/10.1093/nsr/nwab157.
15. Li, N.; Si, D. H.; Wu, Q. J.; Wu, Q.; Huang, Y. B.; Cao, R. Boosting Electrocatalytic CO_2 Reduction with Conjugated Bimetallic Co/Zn Polyphthalocyanine Frameworks. *CCS Chemistry.* **2022,** 0 (0), 1-14. https://doi.org/10.31635/ccschem.022.202201943.
16. Guo, W.; Sun, X.; Chen, C.; Yang, D.; Lu, L.; Yang, Y.; Han, B. Metal-Organic Framework-Derived Indium-Copper Bimetallic Oxide Catalysts for Selective Aqueous Electroreduction of CO_2. *Green Chem*. **2019**, 21 (3), 503–508. https://doi.org/10.1039/c8gc03261k.
17. Qiu, Y. L.; Zhong, H. X.; Zhang, T. T.; Xu, W. B.; Su, P. P.; Li, X. F.; Zhang, H. M. Selective Electrochemical Reduction of Carbon Dioxide Using Cu Based Metal Organic Framework for CO_2 Capture. *ACS Appl. Mater. Interfaces*. **2018**, 10 (3), 2480–2489. https://doi.org/10.1021/acsami.7b15255.
18. Kim, M. K.; Kim, H. J.; Lim, H.; Kwon, Y.; Jeong, H. M. Metal–Organic Framework-Mediated Strategy for Enhanced Methane Production on Copper Nanoparticles in Electrochemical CO_2 Reduction. *Electrochim. Acta* **2019**, 306, 28–34. https://doi.org/10.1016/j.electacta.2019.03.101.
19. Yao, K.; Xia, Y.; Li, J.; Wang, N.; Han, J.; Gao, C.; Han, M.; Shen, G.; Liu, Y.; Seifitokaldani, A. Metal-Organic Framework Derived Copper Catalysts for CO_2 to Ethylene Conversion. *J. Mater. Chem*. *A.* **2020**, 8 (22), 11117–11123. https://doi.org/10.1039/d0ta02395g.
20. Teesdale, J. J.; Pistner, A. J.; Yap, G. P. A.; Ma, Y. Z.; Lutterman, D. A.; Rosenthal, J. Reduction of CO_2 Using a Rhenium Bipyridine Complex Containing Ancillary BODIPY Moieties. *Catal*. *Today*. **2014**, 225, 149–157. https://doi.org/10.1016/j.cattod.2013.10.091.
21. Wang, R.; Kapteijn, F.; Gascon, J. Engineering Metal–Organic Frameworks for the Electrochemical Reduction of CO_2: A Minireview. *Chem. – An Asian J.* **2019**, 14 (20), 3452–3461. https://doi.org/10.1002/asia.201900710.
22. Lu, W.; Wei, Z.; Gu, Z. Y.; Liu, T. F.; Park, J.; Park, J.; Tian, J.; Zhang, M.; Zhang, Q.; Gentle, T.; Bosch, M.; Zhou, H. C. Tuning the Structure and Function of Metal-Organic Frameworks via Linker Design. *Chem. Soc. Rev.*, **2014**, 43, 5561-5593. https://doi.org/10.1039/c4cs00003j.
23. Lv, X. L.; Yuan, S.; Xie, L. H.; Darke, H. F.; Chen, Y.; He, T.; Dong, C.; Wang, B.; Zhang, Y. Z.; Li, J. R.; Zhou, H. C. Ligand Rigidification for Enhancing the Stability of Metal-Organic Frameworks. *J. Am. Chem. Soc*. **2019**, 141 (26), 10283–10293. https://doi.org/10.1021/jacs.9b02947.
24. Braun, E. M.; Steffek, C. D.; Kim, j.; Rasmussen, P.G.; Yaghi, O. M. 1,4-Benzenedicarboxylate derivatives as links in the design of paddle-wheel units and metal–organic frameworks. *Chem*. *Commun*. **2001**, 2532-2533. https://doi.org/10.1039/B108031H.
25. Nam, D. H.; Shekhah, O.; Lee, G.; Mallick, A.; Jiang, H.; Li, F.; Chen, B.; wicks, J.; Eddaoudi, M.; Sargent, E. H. Intermediate Binding Control Using Metal–Organic Frameworks Enhances Electrochemical CO_2 Reduction. *J. Am. Chem. Soc*. **2020**, 142, 51, 21513–21521. https://doi.org/10.1021/jacs.0c10774.
26. Nam, D. H.; Bushuyev, O. S.; Jun, L.; Luna, P. D.; Seifitokaldani, A.; Dinh, C. T.; Arquer, F. P. G.; Wang, Y.; Liang, Z.; Proppe, A. H.; Tan, S. H.; Todorović, P.; Shekhah, O.; Gabardo, C. M.; Jo, J. W.;

Choi, J.; Choi, M.; Baek, S. W.; Kim, J.; Sinton, D.; Kelley, S. O.; Eddaoudi, M.; Sargent, E. H. Metal–Organic Frameworks Mediate Cu Coordination for Selective CO_2 Electroreduction. *J. Am. Chem. Soc*. **2018**, 140, 36, 11378–11386. https://doi.org/10.1021/jacs.8b06407.

27. Zhao, Y.; Zheng, L.; Jiang, D.; Xia, W.; Xu, X.; Yamauchi, Y. Ge, J.; Tang, J. Nanoengineering Metal–Organic Framework-Based Materials for Use in Electrochemical CO_2 Reduction Reactions. *Small*. **2021**, 17(16), 2006590. https://doi.org/10.1002/smll.202006590.
28. Senthil, K. R.; Senthil, K. S.; Anbu K. M. Highly Selective Electrochemical Reduction of Carbon Dioxide Using Cu Based Metal Organic Framework as an Electrocatalyst. *Electrochem*. *commun*. **2012**, 25 (1), 70–73. https://doi.org/10.1016/j.elecom.2012.09.018
29. Hwang, S. M.; Choi, S. Y.; Youn, M. H.; Lee, W.; Park, K. T.; Gothandapani, K.; Grace, A. N.; Jeong, S. K. Investigation on Electroreduction of CO_2 to Formic Acid Using $Cu_3(BTC)_2$ Metal–Organic Framework (Cu-MOF) and Graphene Oxide. *ACS Omega.* **2020**, 5 (37), 23919–23930. https://doi.org/10.1021/acsomega.0c03170.
30. Wu, Y.; Song, X.; Li, S.; Zhang, J.; Yang, X.; Shen, P.; Gao, L.; Wei, R.; Zhang, J.; Xiao, G. 3D-Monoclinic M–BTC MOF (M = Mn, Co, Ni) as Highly Efficient Catalysts for Chemical Fixation of CO_2 into Cyclic Carbonates. *J. Ind. Eng. Chem*. **2018**, 58, 296–303. https://doi.org/10.1016/j.jiec.2017.09.040.
31. De Luna, P.; Liang, W.; Mallick, A.; Shekhah, O.; García De Arquer, F. P.; Proppe, A. H.; Todorović, P.; Kelley, S. O.; Sargent, E. H.; Eddaoudi, M. Metal-Organic Framework Thin Films on High-Curvature Nanostructures Toward Tandem Electrocatalysis. *ACS Appl. Mater*. *Interfaces.* **2018**, 10 (37), 31225–31232. https://doi.org/10.1021/acsami.8b04848.
32. Silva, B. C.; Irikura, K.; Flor, J. B. S.; Santos, R. M. M.; Lachgar, A.; Frem, R. C. G.; Zanoni, M. V. B. Electrochemical Preparation of Cu/Cu_2O-Cu(BDC) Metal-Organic Framework Electrodes for Photoelectrocatalytic Reduction of CO_2. *J. CO_2 Util.* **2020**, 42, 101299. https://doi.org/10.1016/j.jcou.2020.101299.
33. Amirjalayer, S.; Tafipolsky, M.; Schmid, R. Surface Termination of the Metal-Organic Framework HKUST-1: A Theoretical Investigation. *J. Phys. Chem. Lett*. **2014**, 5, 18, 3206–3210. https://doi.org/10.1021/jz5012065.
34. Yoo, D. Y.; Ahmed, I.; Sarker, M.; JinLee. H.; Vinu, A.; HwaJhung, S. Metal–Organic Frameworks Containing Uncoordinated Nitrogen: Preparation, Modification, and Application in Adsorption. *Materials Today*. **2021**, 51, 566-585. https://doi.org/10.1016/j.mattod.2021.07.021.
35. Massolo, E.; Pirola, M.; Benaglia, M. Amide Bond Formation Strategies: Latest Advances on a Dateless Transformation. *EuroJOC*, **2020**, 30, 4641-4651. https://doi.org/10.1002/ejoc.202000080.
36. Wang, X.; Wang, Q.; Wang, Q.; Gao, F.; Gao, F.; Yang, Y.; Guo, H. Highly Dispersible and Stable Copper Terephthalate Metal-Organic Framework-Graphene Oxide Nanocomposite for an Electrochemical Sensing Application. *ACS Appl. Mater. Interfaces.* **2014**, 6 (14), 11573–11580. https://doi.org/10.1021/am5019918.
37. Li, J.; Xia, J.; Zhang, F.; Wang, Z.; Liu, Q. A Novel Electrochemical Sensor Based on Copper-Based Metal-Organic Framework for the Determination of Dopamine. *J. Chinese Chem. Soc*. **2018**, 65 (6), 743–749. https://doi.org/10.1002/jccs.201700410.
38. Rodenas, T.; Luz, I.; Prieto, G.; Seoane, B.; Miro, H.; Corma, A.; Kapteijn, F.; Xamena, F. X. L.; Gascon, J. Metal-Organic Framework Nanosheets in Polymer Composite Materials for Gas Separation. *Nat. Mater*. **2015**, 14 (1), 48–55. https://doi.org/10.1038/nmat4113.
39. Shete, M.; Kumar, P.; Bachman, J. E.; Ma, X.; Smith, Z. P.; Xu, W.; Mkhoyan, K. A.; Long, J. R.; Tsapatsis, M. On the Direct Synthesis of Cu(BDC) MOF Nanosheets and Their Performance in Mixed Matrix Membranes. *J. Memb. Sci*. **2018**, 549, 312–320. https://doi.org/10.1016/j.memsci.2017.12.002.

40. Kubica, P.; Grabczyk, A. W.; Grabiec, E.; Libera, M.; Wojtyniak, M.; Czajkowska, S.; Domański, M. Gas Transport through Mixed Matrix Membranes Composed of Polysulfone and Copper Terephthalate Particles. *Microporous Mesoporous Mater.* **2016**, 235, 120–134. https://doi.org/10.1016/j.micromeso.2016.07.037.
41. Yan, X.; Xu, T.; Chen, G.; Yang, S.; Liu, H.; Xue, Q. Preparation and Characterisation of Electrochemically Deposited Carbon Nitride Films on Silicon Substrate. *J. Phys. D. Appl. Phys.* **2004**, 37 (6), 907–913. https://doi.org/10.1088/0022-3727/37/6/015.
42. Akbari, A.; Sabet, J. K.; Ghoreishi, S. M. Matrimid® 5218 Based Mixed Matrix Membranes Containing Metal Organic Frameworks (MOFs) for Helium Separation. *Chem. Eng. Process. - Process Intensif*. **2020**, 148. https://doi.org/10.1016/j.cep.2020.107804.
43. Elder, A. C.; Aleksandrov, A. B.; Nair, S.; Orlando, T. M. Interactions on External MOF Surfaces: Desorption of Water and Ethanol from CuBDC Nanosheets. *Langmuir.* **2017**, 33 (39), 10153–10160. https://doi.org/10.1021/acs.langmuir.7b01987.
44. Hadjiivanov, K. I.; Panayotov, D. A.; Mihaylov, M. Y.; Ivanova, E. Z.; Chakarova, K. K.; Andonova, S. M.; Drenchev, N. L. Power of Infrared and Raman Spectroscopies to Characterize Metal-Organic Frameworks and Investigate Their Interaction with Guest Molecules. *Chem. Rev.* **2021,** 121, 1286-1424.
45. Sen, R.; Saha, D.; Koner, S.; Brandão, P.; Lin, Z. Single Crystal to Single Crystal (SC-to-SC) Transformation from a Nonporous to Porous Metal–Organic Framework and Its Application Potential in Gas Adsorption and Suzuki Coupling Reaction through Postmodification, Chem. Eur. J. 2015, 21, 5962-5971.
46. Liu, H.; Chu, J.; Yin, Z.; Cai, X.; Zhuang, L.; Deng, H. Covalent Organic Frameworks Linked by Amine Bonding for Concerted Electrochemical Reduction of CO_2. *Chem*. **2018**, 4(7), 1696-1709. https://doi.org/10.1016/j.chempr.2018.05.003.
47. Zheng, W.; Lee, L. Y. S. Metal–Organic Frameworks for Electrocatalysis: Catalyst or Precatalyst? *ACS Energy Lett*. **2021**, 6, 8, 2838–2843. https://doi.org/10.1021/acsenergylett.1c01350.
48. Khalil, I. E.; Xue, C.; Liu, W.; Li, X.; Shen, Y. Li, S. Zhang, W.; Huo, F. The Role of Defects in Metal–Organic Frameworks for Nitrogen Reduction Reaction: When Defects Switch to Features. *Adv. Func. Mater*. **2021**, 31 (17), 2010052. https://doi.org/10.1002/adfm.202010052.
49. Zhang, F.; Zhang, J.; Zhang, B.; Zheng, L.; Cheng, X.; Wan, Q.; Han, B.; Zhang, J. CO_2 Controls the Oriented Growth of Metal-Organic Framework with Highly Accessible Active Sites. *Nat*. *Commun*. **2020**, 11 (1), 1–8. https://doi.org/10.1038/s41467-020-15200-4.
50. Ming, F.; Hou, J.; Huo, D.; Zhou, J.; Yang, M.; Shen, C.; Zhang, S.; Hou, C. Copper-Based Metal-Organic Framework Nanoparticles for Sensitive Fluorescence Detection of Ferric Ions. *Anal*. *Methods.* **2019**, 11 (34), 4382–4389. https://doi.org/10.1039/c9ay01093a.
51. Szanyi, J.; Daturi, M.; Clet, G.; Baer, D. R.; Peden, C. H. F.; Well-studied Cu–BTC still serves surprises: evidence for facile Cu^{2+}/Cu^{+} interchange. *Phys. Chem. Chem. Phys*., **2012**, 14, 4383-4390. DOI https://doi.org/10.1039/C2CP23708C.
52. Ahmad, A.; Robertson, C. M.; Steiner, A.; Whittles, T.; Ho, A.; Dhanak, V.; Zhang, H. Cu(i)Cu(ii)BTC, a microporous mixed-valence MOF via reduction of HKUST-1. *RSC Adv*. **2016**, 6, 8902-8905. https://doi.org/10.1039/C5RA23754H.
53. Wang, D.; Jiang, H.; Tan, J.; Chen, Y.; An, Y.; Chen, Y.; Wu, Y.; Liu, C.; Sun, H.; Liu, J.; Wu, D.; Shen, B. Manipulating Oxidation States of Copper within Cu-BTC Using $Na_2S_2O_3$ as a New Strategy for Enhanced Adsorption of Sulfide. *Ind. Eng. Chem. Res*. **2019**, 58, 42, 19503–19510. https://doi.org/10.1021/acs.iecr.9b04349.
54. Taher, A.; Kim, D. W.; Lee, I. M. Highly Efficient Metal Organic Framework (MOF)-Based Copper Catalysts for the Base-Free Aerobic Oxidation of Various Alcohols. *RSC Adv*. **2017**, 7 (29), 17806–17812. https://doi.org/10.1039/c6ra28743c.

55. Kaur, M.; Mehta, S. K.; Kansal, S. K. Amine-Functionalized Titanium Metal-Organic Framework (NH_2-MIL-125(Ti)): A Novel Fluorescent Sensor for the Highly Selective Sensing of Copper Ions. *Mater. Chem. Phys*. **2020**, 254, 123539. https://doi.org/10.1016/j.matchemphys.2020.123539.
56. Fang, D.; He, F.; Xie, J.; Xue, L. Calibration of Binding Energy Positions with C1s for XPS Results. *J. Wuhan Univ. Technol. Mater. Sci. Ed.* **2020**, 35 (4), 711–718. https://doi.org/10.1007/s11595-020-2312-7.
57. Hori Y. (**2008**) Electrochemical CO_2 Reduction on Metal Electrodes. In: Vayenas C.G., White R.E., Gamboa-Aldeco M.E. (eds) Modern Aspects of Electrochemistry. Modern Aspects of Electrochemistry, vol 42. Springer, New York, NY. https://doi.org/10.1007/978-0-387-49489-0_3.
58. Rashid, N.; Bhat, M. A.; Ingole, P. P. Unravelling the Chemistry of Catalyst Surfaces and Solvents Towards C–C bond Formation Through Activation and Electrochemical Conversion of CO_2 into Hydrocarbons over Micro-structured Dendritic Copper. *Sustainable Energy Fuels*, **2022**, 6, 128-142. https://doi.org/10.1039/D1SE01255J.
59. Deng, D.; Novoselov, K. S.; Fu, Q.; Zheng, N.; Tian, Z.; Bao, X. Catalysis with Two-dimensional Materials and their Heterostructures. *Nature Nanotechnology*. **2016**, 11, 218–230. https://doi.org/10.1038/nnano.2015.340.
60. Wang, H.; Yuan, H.; Hong, S. S.; Lib, Y.; Cui, Y. Physical and Chemical Tuning of Two-dimensional Transition Metal Dichalcogenides. *Chem. Soc. Rev*., **2015**, 44, 2664-2680. https://doi.org/10.1039/C4CS00287C.
61. Chou, T. C.; Chang, C. C.; Yu, H. L.; Yu, W. Y.; Dong, C. L.; Vélez, J. J. V.; Chuang, C. H.; Chen, L. C.; Lee, J. F.; Chen, J. M. Wu, H. L. Controlling the Oxidation State of the Cu Electrode and Reaction Intermediates for Electrochemical CO_2 Reduction to Ethylene. *J. Am. Chem. Soc*. **2020**, 142, 6, 2857–2867. https://doi.org/10.1021/jacs.9b11126.
62. Lee, S. Y.; Jung, H.; Kim, N. K.; Oh, H. S.; Min, B. K.; Hwang, Y. J. Mixed Copper States in Anodized Cu Electrocatalyst for Stable and Selective Ethylene Production from CO_2 Reduction. *J. Am. Chem. Soc.* **2018**, 140, 28, 8681–8689. https://doi.org/10.1021/jacs.8b02173.
63. Bagheri, A. R.; Ghaedi, M. Application of Cu-based Metal-organic Framework (Cu-BDC) as a Sorbent for Dispersive Solid-phase Extraction of Gallic Acid from Orange Juice Samples Using HPLC-UV Method. *Arabian Journal of Chemistry*. **2020**, 13(5), 5218-5228. https://doi.org/10.1016/j.arabjc.2020.02.020.
64. Carson, C. G.; Brunnello, G.; Lee, S. G.; Jang, S. S.; Gerhardt, R. A.; Tannenbaum, R. Structure Solution from Powder Diffraction of Copper 1,4-Benzenedicarboxylate. *Eur. J. In. Chem*. **2014**, 12, 2140-2145. https://doi.org/10.1002/ejic.201301543.
65. Kang, X.; Li, L.; Sheveleva, A.; Han, X.; Li, J.; Liu, L.; Tuna, F.; McInnes, E. J. L.; Han, B.; Yang, S.; Schröder, M. Electro-reduction of Carbon Dioxide at Low Over-potential at a Metal–organic Framework Decorated Cathode. *Nature Comm*. **2020**, 11, 5464. https://doi.org/10.1038/s41467-020-19236-4.
66. Ramos Sende, J. A.; Arana, C. R.; Hernández, L.; Potts, K. T.; Keshevarz, M. K.; Abruña, H. D. Electrocatalysis of CO_2 Reduction in Aqueous Media at Electrodes Modified with Electropolymerised Films of Vinylterpyridine Complexes of Transition Metals. *Inorg. Chem*. **1995**, 34 (12), 3339–3348. https://doi.org/10.1021/ic00116a028.
67. Pugh, J. R.; Bruce, M. R. M.; Sullivan, B. P.; Meyer, T. J. Formation of a Metal-Hydride Bond and the Insertion of CO_2. Key Steps in the Electrocatalytic Reduction of Carbon Dioxide to Formate Anion. *Inorg. Chem*. **1991**, 30 (1), 86–91. https://doi.org/10.1021/ic00001a016.
68. Rashid, N.; Bhat, M. A.; Ingole, P. P.; Dendritic Copper Microstructured Electrodeposits for Efficient and Selective Electrochemical Reduction of Carbon Dioxide into C1 and C2 Hydrocarbons. *Journal of CO_2 Utili*. **2020**, 38, 385-397. https://doi.org/10.1016/j.jcou.2020.02.017.

69. Rashid, N.; Das, A.; Bhat, M. A.; Ingole, P. P.; Unprecedented Lower Over-potential for CO_2 Electro-reduction on Copper oxide Anchored to Graphene Oxide Microstructures. *Journal of CO_2 Uti*li. **2020**, 39, 101178. https://doi.org/10.1016/j.jcou.2020.101178.
70. Su, G. M.; Wang, H.; Barnett, B. R.; Long, J. R.; Prendergast, D.; Drisdell, W. S. Backbonding contributions to small molecule chemisorption in a metal–organic framework with open copper(i) centers. *Chem. Sci.,* **2021,** 12, 2156-21640.
71. Liu, J.; Cheng, L.; Wang, Y.; Chen, R.; Xiao, C.; Zhou, X.; Zhu, Y.; Li, Y.; Li, C. Dynamic determination of Cu^+ roles for CO_2 reduction on electrochemically stable Cu_2O-based nanocubes. *J. Mater. Chem. A,* **2022,** 10, 8459-8465.
72. Ju, W.; Bagger, A.; Hao, G. P.; Varela, A. S.; Sinev, I.; Bon, V.; Roldan Cuenya, B.; Kaskel, S.; Rossmeisl, J.; Strasser, P. Understanding Activity and Selectivity of Metal-Nitrogen-Doped Carbon Catalysts for Electrochemical Reduction of CO_2. *Nat. Commun*. **2017**, 8 (1), 1–9. https://doi.org/10.1038/s41467-017-01035-z.
73. Ponnurangam, S.; Chernyshova, I. V.; Somasundaran, P. Nitrogen-Containing Polymers as a Platform for CO_2 Electroreduction. *Advances in Colloid and Interface Science*. **2017**, 184–198. https://doi.org/10.1016/j.cis.2016.09.002.
74. Lau, G. P. S.; Schreier, M.; Vasilyev, D.; Scopelliti, R.; Grätzel, M.; Dyson, P. J. New Insights into the Role of Imidazolium-Based Promoters for the Electroreduction of CO_2 on a Silver Electrode. *J. Am. Chem. Soc*. **2016**, 138 (25), 7820–7823. https://doi.org/10.1021/jacs.6b03366.
75. Zhang, S.; Kang, P.; Ubnoske, S.; Brennaman, M. K.; Song, N.; House, R. L.; Glass, J. T.; Meyer, T. J. Polyethylenimine-Enhanced Electrocatalytic Reduction of CO_2 to Formate at Nitrogen-Doped Carbon Nanomaterials. *J. Am. Chem. Soc*. **2014**, 136 (22), 7845–7848. https://doi.org/10.1021/ja5031529.
76. Sylvianti, N.; Do, T. T.; Marsya, M. A.; Park, J.; Kang, Y. C.; Kim, J. H. Self-Assembled Poly(4-Vinylpyridine) as an Interfacial Layer for Polymer Solar Cells. Bull. *Korean Chem. Soc*. **2016**, 37 (1), 13–18. https://doi.org/10.1002/bkcs.10613.